Int. J. Heat Mass Transfer. Vol. 14, pp. 1093–1113. Pergamon Press 1971. Printed in Great Britain

AXIAL HEAT TRANSFER IN PACKED BEDS. STAGNANT BEDS BETWEEN 20 AND 750°C

G. S. G. BEVERIDGE

Department of Chemical Engineering, Heriot-Watt University, Edinburgh EH1 1HX, Scotland

and

D. P. HAUGHEY

The Meat Industry Research Institute of New Zealand (Inc.), P.O. Box 617, Hamilton, New Zealand

(*Received* 3 *July* 1970 *and in revised form* 12 *October* 1970)

Abstract—Many industrial applications of random packed beds of solid particles involve axial high temperature heat transfer.

The mechanisms of conduction and radiation have been evaluated independently of convective effects for such systems using a modified geometric model which allows for flux line bending in the solid phase. This model has been used to analyse experimental measurements for heat transfer in a stagnant bed of inert alumina-silicate balls over the temperature range 20–750°C. Comparisons with other theoretical models and experimental data are also made.

NOMENCLATURE

A_i, area available for heat flow;
C, constant;
C_p, specific heat;
D_p, particle diameter;
e, particle surface emissivity;
h, heat transfer coefficient;
H_r, radiation heat transfer dimensionless group $(h_r \beta D_p/k_g)$;
k, thermal conductivity of single phase system;
k_e, effective thermal conductivity of two phase system;
n, number of points of contact per particle;
Nu, Nusselt dimensionless group;
N_{PR}, number of pendular rings in a unit cell;
Q, Q_i, heat flux per unit area;
T, temperature;
V_{PR}, volume of a pendular ring;
X, thermal conductivity ratio (k_s/k_g);
Y, effective thermal conductivity ratio (k_e/k_g);
Y^*, effective thermal conductivity ratio under vacuum;
z, distance;
Z, bed length;
α, ratio, ϕ/β;
α^*, product, $\alpha\varepsilon_{A_2}$;
β, constant defining βD_p the particle layer spacing; number of particle diameters in unit cell length;
ε, bulk mean voidage;
ε_{A_i}, area fraction (see Fig. 4);
θ_p, angle between point to point contacts;
θ_{PR}, angle defining a pendular ring;
σ, Stefan–Boltzmann constant;
ϕ, constant defining ϕD_p the gas layer thickness in gas/solid series path (see Fig. 4);
χ, radiation function.

Subscripts

c, conduction;
g, gas phase;

i, heat transfer path ($i = 1$, gas; $i = 2$, gas/solid; $i = 3$, solid);
0, hot face of bed;
p, point to point contact;
r, radiation;
s, solid phase;
t, solid reference material.

These quantities may be expressed in any set of consistent units.

1. INTRODUCTION

PACKED beds of particulate solids find a central place as a processing tool in a wide variety of physical and chemical operations due to their large surface area and good fluid mixing. Applications include chemical reaction, drying, filtration, distillation, gas absorption, adsorption, leaching, ion exchange and heat regeneration. Many of these involve the transfer of heat between the bed material and the fluid in the bed. An interesting application of a different type is the pebble bed nuclear reactor in which fuel pellets liberate heat to a gas flowing through the bed [1–3].

Particular applications of interest are non-catalytic gas–solid reactions such as zinc sulphide oxidation during the production of zinc, the combustion of solid fuels, blast furnace reduction of iron ore, limestone calcination, and sintering operations. In zinc sulphide oxidation for example, the sulphide pellets are fed on to a travelling grate, air is drawn down through the thin bed and the surface pellets ignited at one end of the bed [4]. The heat liberated by the highly exothermic reaction is then transferred further into the unreacted portion of the bed by conduction, radiation and convection. This raises the unreacted solid to its ignition temperature allowing the reaction zone to be propagated through the packed bed. The rate of propagation is determined by a series of steps involving reaction kinetics, heat transfer and mass transfer (diffusion of reactants to and from the reaction interface, and evaporation of moisture). It is, however, limited by the rate of the slowest step which has been shown, both theoretically and experimentally, to be the transfer of heat ahead of the reaction zone [5, 6].

The design of such processes thus requires some knowledge of the heat transfer characteristics of the bed at the process temperatures and flow rates. The pertinent features include (a) axial heat flows, since these commercial beds are of large diameter with negligible radial heat losses; (b) axial gas flow, counter or co-current with the heat flow; (c) high temperatures and steep temperature gradients (zinc sulphide temperatures reach 1500°C); (d) possible significant temperature differences between solid and gas; and (e) pseudo-steady state conditions due to the relatively slow propagation rates.

Any evaluation or prediction of heat transfer in a packed bed must account for the two-phase nature of the system by examining the contributions of the three basic modes—conduction, convection and radiation. When the gas flows through the bed all three modes contribute to the heat transfer in the form of various mechanisms which interact by a number of series and parallel paths [7–11], while for a stagnant gas conduction and radiation are the significant modes [12–15]. The following potential mechanisms can be identified in the general case:

Conduction mechanisms

1. Conduction through the solid particles.
2. Conduction across the gas in the voids.
3. Conduction across the stagnant gas surrounding the points of contact between particles.
4. Conduction through the points of contact between particles.

Radiation mechanisms

5. Radiation between adjacent particle surfaces.
6. Radiation between particle surfaces seen through more than one void space.
7. Radiation absorption by the gas.

Convection mechanisms

8. Natural convection in the gas.
9. Forced convection solid–gas heat transfer.
10. Forced convection due to bulk flow, turbulent diffusion or mixing of the gas.

The voluminous literature covering heat transfer in packed beds contains little relevant information for the present situation, with apparently no data for gas flow through high temperature beds where radiation is significant. Even at the lower temperatures the contributions of the various mechanisms are not fully understood. Experimental elucidation is difficult since it is not possible to study the various mechanisms independently of each other.

Two general concepts have been used to describe the overall effects of the combined heat-transfer mechanisms, namely the effective heat transfer coefficient and the effective thermal conductivity. The former is not appropriate here since the retaining vessel is essentially absent and in some cases there is no gas flow. The widely used concept of the effective thermal conductivity, k_e, treats the system as homogeneous allowing the Fourier equation for the heat flux, Q, per unit area, to be written

$$Q = -k_e \frac{\partial T}{\partial z}$$

where $\partial T/\partial z$ is the temperature gradient in the axial direction. The many factors which affect heat transfer in this case, as represented by k_e, include gas velocity, gas and solid temperatures, relative directions of gas and heat flow, fluid and solid properties, as well as the bed voidage and structural characteristics. Attention is devoted here to one-dimensional heat flow systems with gas velocity and temperature level as the major variables in a bed of uniform particles. Part I (this paper) deals with axial heat transfer in a packed bed of uniform low conductivity particles and a stagnant, non-flowing gas. This enables conduction and radiation to be studied substantially free of convection effects. Part II extends the study to the case of gas flow through the bed at both low and high temperatures.

2. EXPERIMENTAL SYSTEM [16]

Alumina silicate balls, essentially spherical at 6 mm dia., were randomly packed in a 300 mm × 150 mm dia. vertical cylindrical container. This bed, with a voidage of 0·399, was open top and bottom and air could be passed upwards if required (Part II of this paper). A set of parallel silicon carbide heating elements provided a heat source at the lower end of the bed. The heat source was insulated radially with refractory bricks but special care had to be taken around the bed itself to obtain radial adiabaticity. This was partly achieved by surrounding the test bed by a 36 mm wide annular guard bed formed from identical particles, through which air could flow if necessary at the same air flow as in the test bed. The rigid test and guard bed containers were built up of thin layers of Fiberfrax* which could withstand 1200°C and had a low thermal conductivity (k_s = 0·072–0·155 W/m°K) preventing axial disturbances. Radial losses were further minimized by surrounding the guard section with a 175 mm wide annulus of magnesium oxide powder containing a multi-sectioned resistance wire heater. The heat flux through the bed containing stagnant gas was determined from the axial temperature gradient in an adiabatic block of known thermal conductivity placed on top of the test/guard bed. The most suitable material was high temperature refractory brick of known thermal conductivity–temperature characteristics. A 110 mm thick slab, 530 mm dia., was prepared by cutting and cementing in chromel–alumel thermocouples. The resulting temperature profiles for a particular heat flux were linear and reproducible, with no radial variation over the test bed diameter.

Solid particle temperatures were measured throughout the bed by thermocouples located at 65 known radial and axial positions. All hot

* Carborundum Co. Ltd.

junctions were placed within specially formed balls before firing and the 0·2 mm unsheathed thermocouple wires were taken out of the bed along separate isothermal paths. During any experiment, once steady state conditions were attained in the bed and the axial heat sink, the local wall heaters were adjusted until the temperatures measured by each of the individual thermocouples along a radius at each height were equal. This took between 3 and 7 days after which the solid particle temperature distribution was recorded. Heat flux readings were also taken in most runs.

3. EXPERIMENTAL RESULTS

Temperature profiles. The steady state temperature readings for various stagnant bed conditions are shown in Fig. 1, profiles being drawn through them as smooth curves. Bed inlet temperatures (hot face values) up to 780°C were investigated and the profiles were reproducible to within 5 per cent.

Heat flow rates. Since there is no radial temperature variation, the heat flux can be considered as solely axial. The flux per unit area, Q, is then obtained from $Q = -k_t(\partial T/\partial z)_t$ where $(\partial T/\partial z)_t$ is the gradient given by the least squares linear profile in the heat flux reference material of thermal conductivity, $k_t = 0{\cdot}206 + 0{\cdot}00026T_t$ W/m°K [17]. Here k_t was evaluated at the mean temperature of the material, T_t. Values of Q are plotted against the hot face temperatures, T_0, in Fig. 2a. The effect of radiation is apparent at the higher temperatures where the curve becomes non-linear.

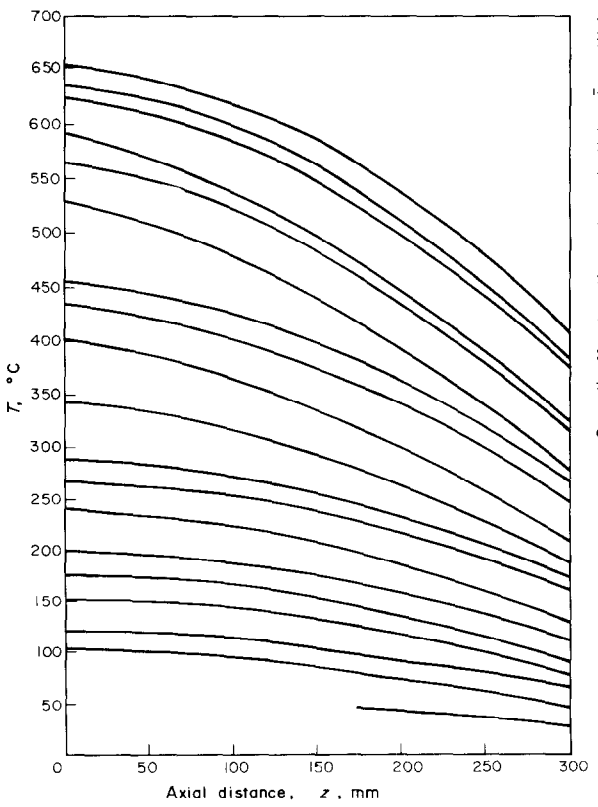

FIG. 1. Stagnant bed temperature profiles, taken using a heat flow meter.

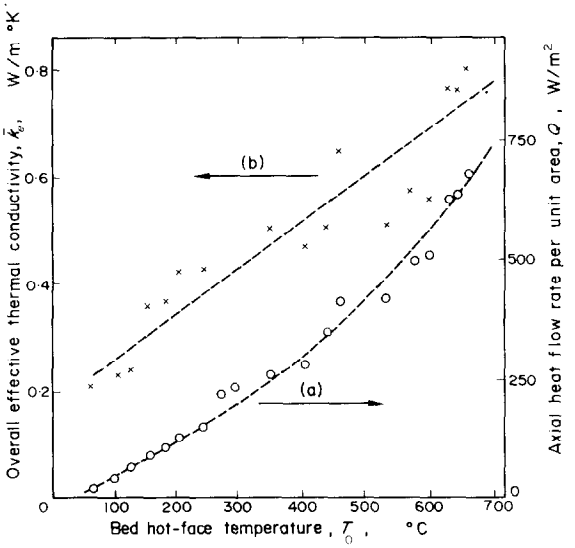

FIG. 2. (a) Stagnant bed axial heat flow rates, Q, as a function of hot end temperature, T_0.
(b) Overall effective thermal conductivity, $\bar{k}_e$, as a function of hot end temperature, T_0.

Overall effective thermal conductivity $\bar{k}_e$. This is defined as $\bar{k}_e = QZ/(T_0 - T_m)$ where $T_0 - T_m$ is the overall temperature drop along the bed of length Z. Any local thermal conductivity variation with axial temperature change through the bed will be averaged out in the value of $\bar{k}_e$. The

$\bar{k}_e$ values thus derived from Figs. 1 and 2a are also presented in Fig. 2b as a function of the hot face temperature, T_0. They increase with temperature, as would be expected, but there is appreciable scatter partly due to the inclusion of such end effects in the bed as radiation from the supporting base plate.

Local effective thermal conductivity k_e. The local coefficient, k_e, may be defined as $k_e = -Q/(\partial T/\partial z)$ in terms of the local bed temperature gradient. The latter can be obtained graphically from large scale plotting of the temperature profiles. The linear plots of the derived gradient against heat flux derived from Figs. 1 and 2a show little effect of Q or $\partial T/\partial z$ on k_e over the range studied. The k_e values then obtained from a least squares fit are presented in Fig. 3 as a function of the local solid particle temperature. Some of the k_e values shown in Fig. 3 were obtained from temperature profile measurements taken without the heat flow meter in position. The values of Q were then determined indirectly [16]. These conditions of an open-ended bed are equivalent to those for the gas flow runs reported in Part II. The effect of the radiation mechanisms is apparent from the non-linearity of the curve which becomes increasingly significant above about 200°C.

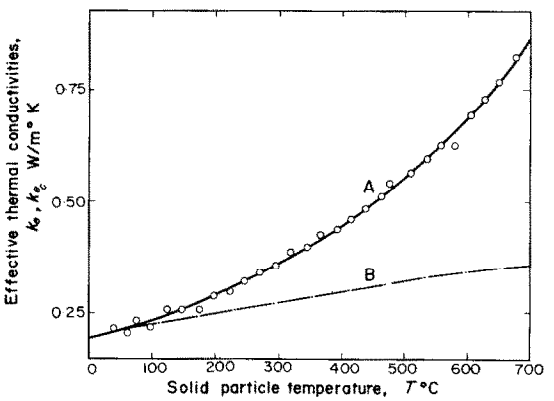

FIG. 3. Effective thermal conductivity as a function of solid particle temperature. (a) Experimental local values, k_e; (b) values, k_{e_c}, predicted by the conduction model of Appendix 1.

4. THEORY

Any analysis of heat transfer in a stagnant packed bed under the present conditions must account for contributions from both conduction and radiation. Let us, however, initially examine a conduction model as a basis for the later incorporation of the radiation effects.

Conduction heat-transfer model

Only conduction (mechanisms 1–4 above) needs to be considered when there is no gas flow (eliminating forced convection), sufficiently small particles (negligible natural convection) and sufficiently low temperatures (negligible radiation). Under these conditions, the effective thermal conductivity, k_e, is primarily dependent on the thermal conductivities of the solid particle and the stagnant gas, k_s and k_g respectively, and the structure of the bed [18–20]. The important factors in the structure which will affect heat transfer are likely to be the voidage, both local and bulk mean (as a measure of the volume concentration of the two phases), and the shape and orientation of the particles (as this will affect the relative positions of the phases and the solid–solid contact points).

Various models have been published to account for the four conduction mechanisms, although not all can specifically account for the point to point contact (mechanism 4), or distinguish between the gas routes (2 and 3). Most of these models as indicated below describe the heterogeneous system in terms of its fluid and solid phase elements arranged in some regular array, with possible adjustment of the voidage to correspond with the application.

The simplest models take an average of the separate phase contributions. Thus, postulating that the conduction through the solid (mechanism 1) acts over a solid volume, $1 - \varepsilon$, and the conduction across the gas in the voids and the stagnent gas round the points of contact (mechanisms 2 and 3) act over a gas volume, ε, an arithmetic mean corresponding to a parallel arrangement of the two phases (Fig. 4a) gives

$$Y_c = \frac{k_{ec}}{k_g} = \varepsilon + (1 - \varepsilon) X.$$

Here Y_c is a dimensionless conduction ratio, X is the ratio of solid to gas conductivities, k_s/k_g, and ε the bulk mean voidage of the bed. A

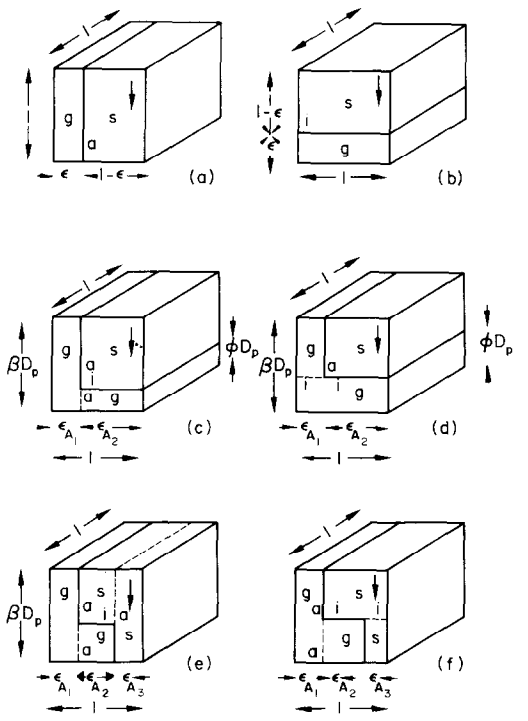

FIG. 4. Unit cell models representing a packed bed containing stagnant gas. a—adiabatic plane, i—isothermal plane, g—gas phase, s—solid phase, → direction of heat flow.

harmonic mean which corresponds to a series arrangement of the phases (Fig. 4b) yields

$$Y_c = \frac{X}{\varepsilon X + (1 - \varepsilon)}.$$

In all practical cases some intermediate form will hold, the geometric mean

$$Y_c = X^{(1-\varepsilon)}$$

having been suggested [21–24] to represent the degree of randomness involved. The parallel and series limits have also been used to provide a model containing two experimentally determined statistical parameters [25, 26], although the mathematical basis has been criticized [27].

In attempting the formulation of more realistic models, it has been found for regular packings of equal spheres [11, 28] that

$$Y_c = 1 - \frac{\pi}{4} + \frac{\pi}{2}\left(\frac{X}{X-1}\right)^2\left(\ln X - \frac{X-1}{X}\right)$$

for cubic, with similar expressions for expanded cubic [29], cubic bounded by paraboloids [30], orthorhombic [31, 32], and tetrahedral [11]; Rayleigh [33] proposing for any such regular packing that

$$Y_c = 1 - 3(1-\varepsilon)\left[\frac{2+X}{1-X} + 1 - \varepsilon - \frac{1-X}{X+\frac{4}{3}} C(1-\varepsilon)^{10/3} + \ldots\right]^{-1}$$

where $C = 1{\cdot}31$ (cubic), $0{\cdot}129$ (body-centred cubic), $0{\cdot}075$ (face-centred cubic) [34]. Other generalized forms have been proposed [35, 36].

For random packings, which are those normally encountered, models have been suggested using unit elements or cells of regular packings, for example, close packed tetrahedral spheres [37] and also interpolations between the thermal conductivity values for different regular packings [28]. The packing of cylinders and cubes has also been considered [28, 29, 33, 38–40], while expressions of the form

$$Y_c = [2\varepsilon + X(3 - 2\varepsilon)](3 - \varepsilon + X)^{-1}$$

have been used [41] on the basis of a random distribution of solid spheres in the continuous medium, and have been extended to the cases of more than one dispersed phase [34, 42–47] and a size distribution of particles [48].

In such 3-dimensional models there is essentially a representative element which is repeated throughout the packing. In an expanded cubic packing [29], for example, the unit cell is a cube containing a quarter of a solid phase spherical element. Although flux lines must bend, the concept of a unit cell has been introduced by assuming effectively one dimensional heat fluxes

and replacing the spherical element of solid by a cube. This concept leads us to various forms of idealized geometric arrangement based on the simple models of Figs. 4a and b. Thc basic geometric cell is that of Fig. 4c with a cell of unit area perpendicular to the heat flow and height equal to the particle layer thickness, βD_p [20]. Heat flow is one dimensional in parallel paths, which are insulated from each other, and the distribution of the two phases is handled only by a two dimensional variation. This system then gives [10, 13, 49–51]

$$Y_c = \varepsilon_{A_1} + \frac{(1 - \varepsilon_{A_1})X}{\alpha X + 1 - \alpha}$$

where $\alpha = \phi/\beta$ and $\varepsilon_{A_1} = (\varepsilon - \alpha)/(1 - \alpha)$. The various models proposed differ in their evaluation of α, β and ε_{A_1}, not all being correctly defined [16].

Modifications include that illustrated in Fig. 4d which gives [32]

$$Y_c = \left[\alpha + \frac{1 - \alpha}{\varepsilon_{A_1} + X(1 - \varepsilon_{A_1})}\right]^{-1}$$

where $\alpha = 1 - [(1 - \varepsilon)/\delta]^{\frac{1}{2}}$, δ being a shape factor, and one [52] based on a set of solid–gas layers in series followed by a group of solid–gas layers in parallel.

These models do not however take into account the point to point contact resistance (mechanism 4). This problem has been extensively discussed for powders [53]. The resistance might be included [54] as an equivalent conductivity, k_p, such that $k_{e_c} = k'_{e_c} + k_p$ where k'_{e_c} is the value based on a model which neglects this mechanism and k_p is related to k_s and ε, although it erroneously implies that the contact resistance is in series with the combined mechanisms 1, 2 and 3, with no allowance for particle loading, deformation and the surface characteristics. Another approach [13] uses an equivalent heat transfer coefficient, h_p, accounting for a heat transfer contact resistance in parallel with the gas phase portion of the gas–solid series mechanism, yielding

$$Y_c = \varepsilon_{A_1} + \frac{(1 - \varepsilon_{A_1})X}{1 - \alpha + \alpha X/(1 + h_p D_p \alpha/k_g)}.$$

For unconsolidated packings h_p has been taken as zero while, based upon a packing of truncated spheres [55], the vacuum thermal conductivity ratio, Y_c^*, has been found to be

$$Y_c^* = X/(C + (\ln 2C)/\pi)$$

where C is defined by CD_p, the contact diameter, and used in analysing a soldered bed of metal spheres [56]. The logical extension is the inclusion of the contact resistance in the idealized cell model as a solid heat flux path (represented by an area fraction ε_{A_3}) arranged parallel to the gas path (Fig. 4e), giving

$$Y_c = \varepsilon_{A_1} + \frac{\varepsilon_{A_2} X}{\alpha X + 1 - \alpha} + \varepsilon_{A_3} X.$$

A more realistic development (Fig. 4f) is introduced here to allow some relaxation of the restriction of no flux line bending. Since some bending will occur, especially in the solid phase [57], this can be partially taken into account by removing the adiabatic boundary between the two parallel paths within the solid phase and inserting an isothermal boundary, as will be seen from comparison of Figs. 4e and f. This yields [Appendix 1, equation A.4e]

$$Y_c = \varepsilon_{A_1} + \left[\frac{1 - \alpha}{X(1 - \varepsilon_{A_1})} + \frac{\alpha}{\varepsilon_{A_2} + X\varepsilon_{A_3}}\right]^{-1}$$

in which $\sum_1^3 \varepsilon_{A_i} = 1$, reducing to

$$Y_c^* = X\left[\frac{1 - \alpha}{1 - \varepsilon_{A_1}} + \frac{\alpha}{\varepsilon_{A_3}}\right]^{-1}$$

for vacuum conditions. A major difference between this and the previous models lies in the derivation of the parameters. As shown in Appendix 2, Y_c is a function of only X, ε and ε_{A_3}, the variation being shown in Figs. 5 and 6. Y_c and Y_c^* both increase monotonically with increasing X (Fig. 5) and ε_{A_3} (Fig. 6), the effects being greater for vacuum. In particular in Fig. 5 the increase in Y_c^* with X is linear, while for

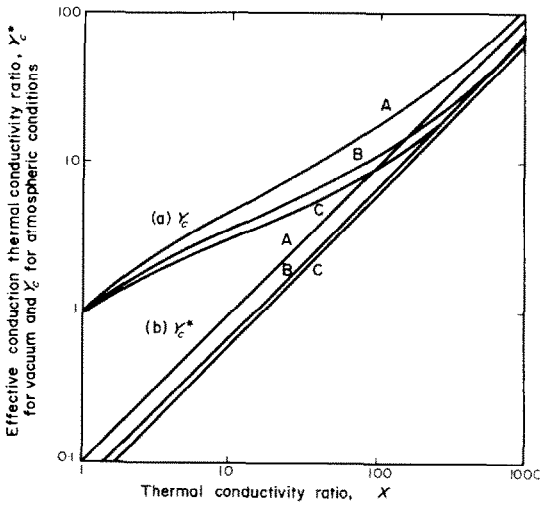

FIG. 5. Effect of the phase conductivity ratio, X, and the bed voidage, ε, on the effective thermal conductivities predicted by a conduction model under (a) atmospheric conditions —Y_c and (b) vacuum —Y_c^* when $\varepsilon_{A_3} = 0{\cdot}01$. Parameter is bed voidage, ε; curves A: 0·26, B: 0·40, C: 0·50.

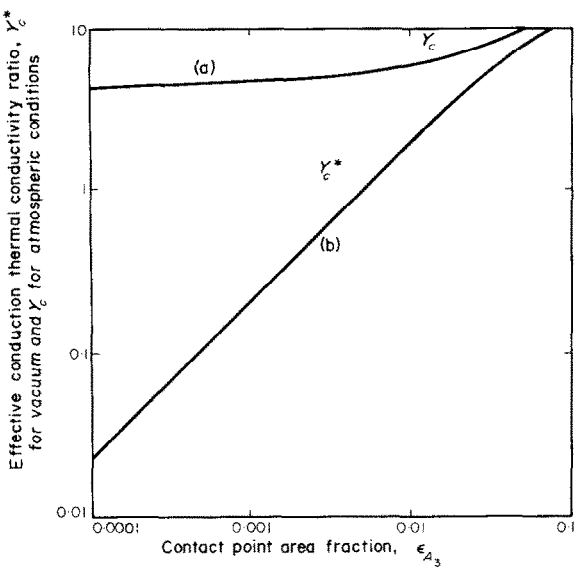

FIG. 6. Effect of contact point area fraction, ε_{A_3}, on the conduction model prediction of effective thermal conductivities under (a) atmospheric—Y_c and (b) vacuum conditions—Y_c^*, for a given bed voidage, $\varepsilon = 0{\cdot}40$, and a given phase thermal conductivity ratio, $X = 30$.

both Y_c and Y_c^* there is a linear decrease over the range of 0·26–0·50 in ε which corresponds to the usual range of values in a packed bed.

While X and ε are definable physical properties, the parameter, ε_{A_3}, which can be related to a contact area angle, θ_p (see Appendix 2), must be determined experimentally even for a given set of particles, since it will be affected by the particle loading and deformation as well as the surface characteristics of the solid. If this model is used under conditions other than for vacuum or atmospheric pressure the effect of pressure on the thermal conductivity of the gas, k_g, must be evaluated from the kinetic theory of gases [51, 58].

Our proposed geometric model differs from the others described above in that the contact point path of area ε_{A_3} is not insulated adiabatically in a radial direction from the series solid path of area ε_{A_2} (compare Figs. 4e and f). The bending of the isothermal lines in the detailed work of Deissler and Boegli [57] shows that heat must cross the boundary between these paths. Under vacuum conditions the previous models with an adiabatic line (for example, Fig. 4e) allow heat transfer to occur only through the solid contact point path. In fact, heat transfer takes place throughout the solid and the greater the number of contact points the more uniform is the flux distribution through the particles. The present model under vacuum conditions allows for this by allowing heat to initially flow through a solid area $\varepsilon_{A_2} + \varepsilon_{A_3}$ over a length $(\beta - \phi)D_p$ and then to flow out into the next cell through the solid contact area ε_{A_3}.

Conduction and radiation heat transfer model

Although radiant heat transfer will occur only through the voids of a packed bed of opaque solid, pseudo-homogeneous models have been proposed which consider the solid and the gas as a single homogeneous medium. The numerical solution of the resultant differential or integro-differential equations for conduction and radiation in absorbing and scattering models has been extensively examined [59–65]. Analytical solutions were found in a few simple cases [66–68], thus from the boundaries of an optically thick bed [68]

$$Y_r = \frac{k_{e_r}}{k_g} = \frac{8\sigma T^3}{k_g(a + 2b)}$$

where a and b are absorption and scattering cross-sectional areas per unit volume.

The radiation contribution has also been used combined with a geometric model [69] or calculated from a random walk interpretation [70], the latter giving

$$Y_r = \frac{4D_p T^3}{3k_g}.$$

The simplest radiation geometrical model however, and the only justifiable one at this stage, is that with two radiating plane surfaces, the heat flux per unit area being represented (when planes are of respective temperatures T_1 and T_2) by

$$Q_r = \chi\sigma(T_1^4 - T_2^4)$$

where the view factor and emissivity function χ can take different forms (Appendix 4). Since the heat flux can be related to a radiation thermal conductivity, k_r, and to a radiation heat transfer coefficient, h_r, by

$$Q_r = -k_r \frac{\partial T}{\partial z} = h_r(T_1 - T_2)$$

we can thus say* that

$$k_r/\beta D_p = h_r = 4\chi\sigma T^3$$

when $T_1 - T_2$ is small compared to the absolute value of $T(= T_1)$.

The parameters in these models have a highly complex interaction with the structural and physical properties of the bed, and for this reason there is little justification in representing the radiation mechanism other than by adding suitable terms to the simplest model such as the geometrical conduction models of Fig. 4. Thus Schotte [14] used an analysis similar to that of Argo and Smith [12] accounting for both the radiation between adjacent particle surfaces (mechanism 5) and the radiation between particle surfaces seen through more than one void space (mechanism 6) giving

$$Y_r = \varepsilon X_{r_g} + \frac{1 - \varepsilon}{\frac{1}{X} + \frac{1}{X_{r_s}}}$$

where here $X_{r_s} = X_{r_g}(= h_r D_p/k_g = 4D_p\chi\sigma T^3/k_g)$, with $\chi = e$, the thermal conductivity in the packed bed being then given by $Y = Y_c + Y_r$. In fact there is an interaction between the radiation and other heat transfer mechanisms and the contribution Y_r cannot be added simply to the conduction terms. It is more satisfactory to utilize h_r within the conduction type model (Fig. 4e) getting, for example [10, 13, 49],

$$Y = \varepsilon_{A_1}(1 + X_{r_g}) + \frac{\varepsilon_{A_2}}{\frac{\alpha}{1 + \alpha X_{r_s}} + \frac{1 - \alpha}{X}} + \varepsilon_{A_3} X.$$

Normally no distinction is made between mechanisms 5 and 6 as represented by the Nusselt numbers X_{r_s} and X_{r_g} respectively although Yagi and Kunii [10] in fact used $X_{r_s} \neq X_{r_g}$, but let $\chi_s = e/(2 - e)$ and

$$\chi_g = \left[1 + \frac{\varepsilon(1 - e)}{2(1 - \varepsilon)e}\right]^{-1}.$$

Our present model results in the expression (Appendix 3, equation A.7)

$$Y = \frac{k_e}{k_g} = \varepsilon_{A_1}(1 + H_r) + \frac{1}{\frac{1 - \alpha}{X(1 - \varepsilon_{A_1})} + \frac{\alpha}{\varepsilon_{A_2}(1 + H_r) + X\varepsilon_{A_3}}}$$

---

* Since

$$T_1^4 - T_2^4 = T_1^4\left[1 - \left(\frac{T_2}{T_1}\right)^4\right] = T_1^4\left[1 - \left(1 - \frac{\Delta T}{T_1}\right)^4\right]$$

$$= T_1^4\left[1 - \left(1 - \frac{4\Delta T}{T_1} + \ldots\right)\right] \approx 4T_1^3\Delta T,$$

if $\Delta T(= T_1 - T_2) \ll T_1$, then

$$Q_r = \chi\sigma(T_1^4 - T_2^4) \approx 4\chi\sigma T_1^3(T_1 - T_2)$$

which defines h_r. Similarly $\partial T/\partial z \approx -\Delta T/\beta D_p$ to define k_r.

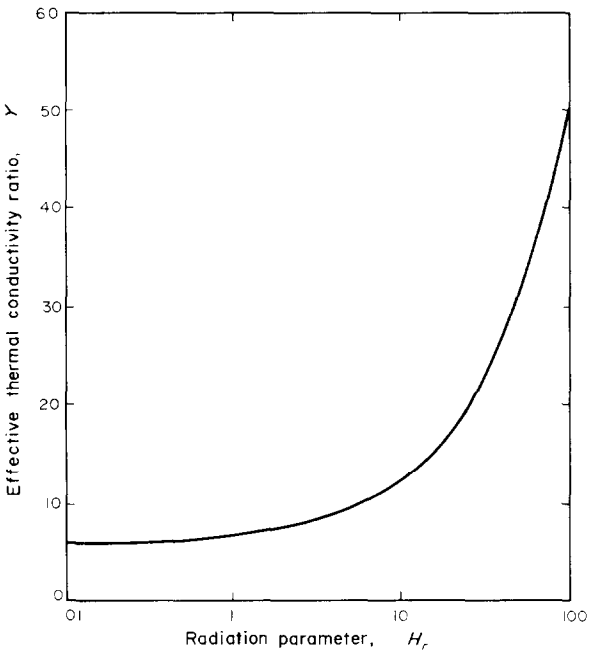

FIG. 7. Effect of the radiation parameter, H_r ($= h_r \beta D_p / k_g$), on the effective thermal conductivity ratio. Y, predicted by the conduction–radiation model for the system $\varepsilon = 0{\cdot}40$, $X = 30$, $\varepsilon_{A_3} = 0{\cdot}01$.

where $H_r = k_r/k_g = \beta h_r D_p / k_g$, the variation of Y with H_r being shown in Fig. 7.

5. ANALYSIS

A comparison of Figs. 2b and 3 indicates the unsatisfactory nature of any analysis based on overall data. Overall thermal conductivities introduce a high degree of scatter into the analysis due to the need for an averaging which must include wide ranges of operating temperatures as well as including various inhomogeneities due to end effects. The present analysis will be based only on locally derived coefficients which, as shown in Fig. 3, agree well with each other.

Conduction mechanism

The present conduction model (Appendix 1) can be used to evaluate the relative contributions of the different conduction mechanisms and to predict the thermal conductivity over a range of of temperature. Figure 8 indicates the relationship of this model to some other models which neglect the point contact. The large variation at high values of k_s will be obvious, the present model being the only one which approaches the value imposed by the upper limit of the parallel phase model as would be expected at high X values. Masamune and Smith's [51] model gives similar results. Further comparisons for the present experimental system data are shown in Figs. 9 and 10. The wide variation between models is noticeable especially when the point contact resistance is neglected (Fig. 10).

Predictions for the present experimental system can be obtained if the thermal conductivities of the solid and gas and the bed voidage are known, together with information on the contact resistance, ε_{A_3}. The solid thermal conductivity, k_s, was measured by the ball com-

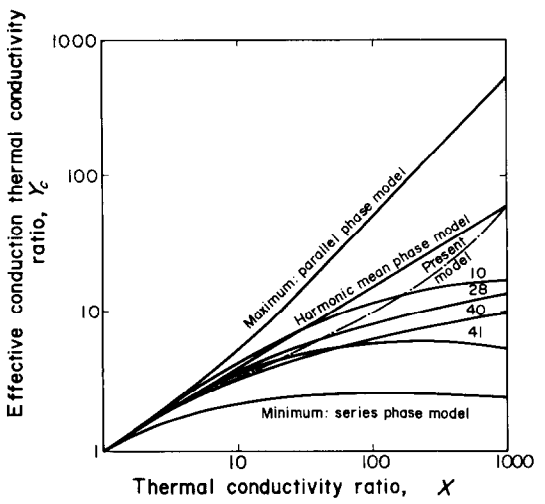

FIG. 8. The variation of effective thermal conductivity predictions for random packings of voidage 0·40, not accounting for contact point resistance. Parameters refer to reference source list.

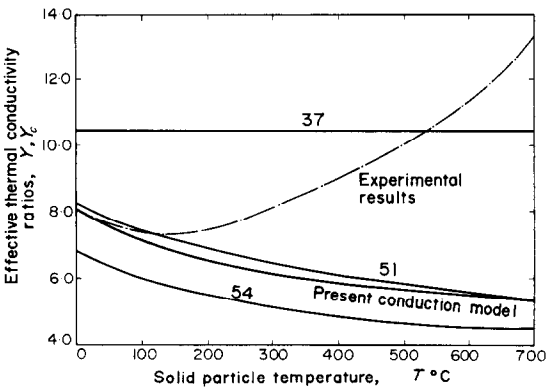

FIG. 9. Comparison of experimental and predicted conduction values of the effective thermal conductivity ratios, Y and Y_c respectively, using models which include the contact point resistance. Parameters refer to reference source list.

parator method [71, 72] and found* within 10 per cent to be 1·38 W/m°K at 20°C. Its variation with temperature was assumed to be similar to the variation for a porcelain [73] of the same composition, yielding $k_s = 1{\cdot}37 + 0{\cdot}00037\ T$ where T is in °C. Using published

* Acknowledgement is made to Dr. Gordon, University of Glasgow, for the measurements.

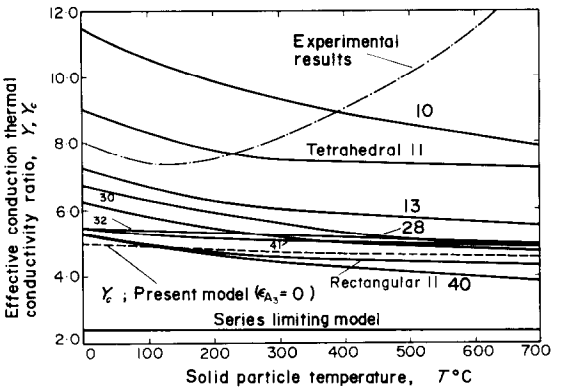

FIG. 10. Comparison of experimental and predicted conduction values of the effective thermal conductivity ratios, Y and Y_c respectively, using models which do not allow for contact point conduction. Parameters refer to reference source list.

variations of k_g [74] this is equivalent to a range of X from about 58 to 25 over 20–700°C.

For a bed voidage of $\varepsilon = 0{\cdot}40$, the following parameters can be estimated from the equations derived in Appendix 2, $n = 6{\cdot}714$, $\theta_{PR} = 42° 36'$, $\alpha^* = 0{\cdot}09245$, $\varepsilon_{A_1} = 0{\cdot}3076$ and $\varepsilon_{A_2} + \varepsilon_{A_3} = 0{\cdot}6924$. Using the experimental value of $Y_c = 8{\cdot}02$, derived from Fig. 3, and the appropriate X value, it can thus be found that $\varepsilon_{A_3} = 0{\cdot}010$ so that $\alpha = 0{\cdot}1355$. This then results in the specific relation

$$Y_c = 0{\cdot}3076 + \frac{1}{\dfrac{1{\cdot}248}{X} + \dfrac{0{\cdot}1355}{0{\cdot}6823 + 0{\cdot}010\,X}}$$

a monotonic decreasing function of temperature (Fig. 9) due to the strong temperature dependence of X. The alternative approach would be the evaluation of ε_{A_3}, using vacuum values of Y [51]. The contribution of each conduction mechanism to the total flow through this system can thus be predicted. It is seen in Table 1 that, for example, the gas parallel path accounts for less than 6 per cent and might well be neglected. The gas series fraction of the combined flow is much more important than the point contact, its effect increasing in the higher temperature range. Other published conduction models can also be used to predict the data for the present

Table 1. Relative contributions of the various mechanisms, showing fraction of total heat flow through specific path

Mechanism*		Neglecting radiation			Including radiation		
		0	300	700°C	0	300	700°C
Solid–gas series:	$1 - \varepsilon_{A_1}(1 + H_r)/Y_c$	0·963	0·951	0·943	0·963	0·818	0·542
Gas series		0·522	0·683	0·692	0·522	0·435	0·171
Point contact		0·441	0·268	0·251	0·441	0·218	0·062
Intra cell radiation		—	—	—	0	0·165	0·309
Intercell radiation	$\varepsilon_{A_1} H_r/Y_c$	—	—	—	0	0·134	0·426
Gas parallel path	ε_{A_1}/Y_c	0·037	0·049	0·057	0·037	0·048	0·032
Gas radiation	—	—	—	—	0	0	0

* See equation (A.7), appendix 3.

experimental system, shown in Fig. 9 for models which include a point contact resistance, and in Fig. 10 for those in which it is ignored. While comparison with experimental data is only valid at low temperatures, the general fit is not particularly satisfactory.

The present model has been found to predict previously published results (Table 2) with some confidence, using thermal conductivity measurements taken under vacuum in the lower temperature range. Table 2 shows that the predicted values agree very closely with those actually measured for atmospheric conditions. The published data obtained with unsteady state methods [24, 40] did not in general show good agreement with either the steady state experimental results on the same materials or with the conduction model. This is probably because contact between the particles and the heat-transfer surface has a significant effect on the results under unsteady state conditions especially under vacuum. Figure 11 shows the values of the contact angle, θ_p, obtained by examining published thermal conductivity data at atmospheric pressure, extrapolated to 0°C. The scatter of the data points cover the range $\varepsilon = 0{\cdot}38$–$0{\cdot}50$ and $X = 4{\cdot}5$–8400 indicating the significant effect of the surface characteristics and loading of the particles on the point contact resistance, and the impossibility of their prediction.

Table 2. Comparison of published data (axial [51] and radial [75] steady state data) with present conduction model predictions for random packed beds of spheres

System	Temperature (°C)	X	ε	Experimental Y*	Predicted Y_c	Experimental Y	Reference
Glass spheres $2{\cdot}9$–47×10^{-3} cm. dia.	40–44	38·53	0·38	1·913	6·40	6·62	51
Stainless steel shot $7{\cdot}1 \times 10^{-3}$ cm.	40–44	600·0	0·265	0·639	9·36	9·26	51
Glass powder	0–1·5	44·9	0·35	1·31	6·65	6·62	75

Conduction and radiation mechanisms

The present model extended to include the radiation mechanisms (Appendix 3) can also be used to evaluate these mechanisms once

measurements of the effect of local thermal conductivities have been obtained for the stagnant bed, radiation absorption by the gas (mechanism 7) being neglected. The previously determined conduction parameters on substitution then yield the specific relation for the present system

$$Y = 0{\cdot}3076(1 + H_r) + \frac{1}{\frac{1{\cdot}248}{X} + \frac{0{\cdot}1355}{0{\cdot}6823(1 + 0{\cdot}1355H_r) + 0{\cdot}010X}}$$

This can be used to predict the variation of the thermal conductivity if the temperature variations of X and H_r are known. As will be seen below, the radiation parameter, H_r, is not predictable in the present situation, but can be determined only by comparison of calculated and experimental values of Y. The marked temperature dependence of H_r is seen from Fig. 12. From this it is found that h_r is proportional to $T^{3{\cdot}64}$ above 250°C. The apparent discrepancy below 250° is resolved by back calculation in which it is found for example that at 0°C this relation would give $H_r = 0{\cdot}39$ compared to the assumed value of 0. This new

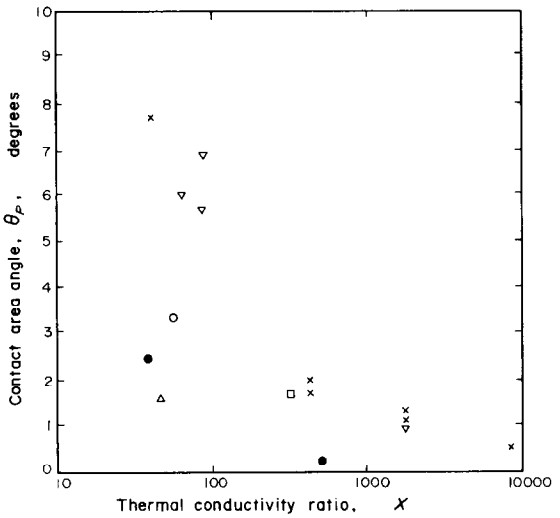

FIG. 11. Contact area angles, θ_p, for random packed beds of spheres of bed voidages $\varepsilon = 0{\cdot}38$–$0{\cdot}50$. ○ present data [16], × [11], □ [69], ▽ [10], △ [75], ● [51].

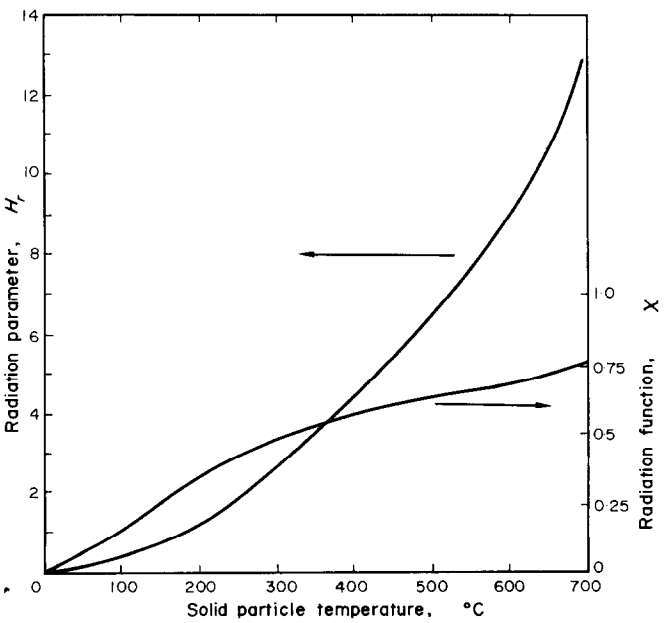

FIG. 12. Experimental values of the radiation parameter, H_r ($= h_r \beta D_p / k_g$), and function, χ, for the stagnant bed.

value however would only make a 2 per cent error in the estimated value of Y given in Fig. 7. Since the radiation heat-transfer coefficient can be written as $h_r = 4\chi\sigma T^3$ this implies that χ, which is also shown in Fig. 12 for $\beta = 0{\cdot}8756$ and is equal to the product of an emissivity function and a view factor, has a temperature dependence of $T^{0{\cdot}64}$. Since the emissivity function has a typical form such as $e/(2-e)$, $e^2/2\ldots$ it will be a decreasing function of temperature because the solid emissivity, e, is approximately [76] inversely proportional to T above 300°C. This indicates that radiation scattering will increase the value of the view factor at increased temperatures. Any more detailed analysis, using more complex radiation models [15, 68, 69], would require further knowledge of the radiation absorption, scattering and transmission parameters than is available for the present experiments.

The results from the derived model for the present system can now be used to determine the resultant contributions of the conduction and radiation mechanisms as shown in Table 1. At 700°C the radiation paths account for some 73 per cent of the heat flux, although the combined gas–solid path is still the most important contribution. The contribution of the point contact has now decreased from about 44 per cent to 6 per cent.

A slightly modified version of the radiation model was also tested. In this the top plane of the gas conduction parallel path of area ε_{A_1} radiated to the side wall of the solid section of length $(\beta - \phi)D_p$, with a radiant flux $h_{r_g}(T_1 - T_2)$. The result is the multiplication of the $(1-\alpha)/[X(1-\varepsilon_{A_1})]$ term by the factor $(\tanh m)/m$ where

$$m^2 = \frac{(1-\alpha)^2\beta D_p}{(1-\varepsilon_{A_1})}\frac{H_r}{X}.$$

For the situation considered here, $m = 0{\cdot}1046$ if β is taken as 0·8756 [19] so that the modification factor has its greatest value of 1·004 at 700°C implying that the modification is insignificant. This would appear to support the assumption that the same form of h_r can be used here to represent both mechanisms 5 and 6.

The experimental data represented by the above relation are in fact mean local thermal conductivity values. The probability distribution of the local effective thermal conductivity can be found [16] at any temperature using the parameters α, ε_{A_1}, ε_{A_2}, ε_{A_3} together with a probability distribution of the local mean voidage [18, 19]. The higher temperature levels result in the smoothing out of the local variations.

Values of the radiation parameter, H_r, were derived by applying the present conduction-radiation model to the experimental results available in the literature for the effective thermal results available in the literature for the effective thermal conductivities of random packed beds of spheres. The trends were consistent, showing a monotonic increase with temperature (as for the present experimental results shown in Fig. 12), although the results with aluminium and glass showed a greater temperature dependence. In attempting to determine the effect of other factors such as particle size and emissivity, derived values of $\beta\chi$ are presented in Fig. 13. Since the layer spacing represented by β will be a constant, this graph will thus represent the temperature variation of the radiation function χ. Although the scatter between experimental systems is quite wide, the results are similar, the general trend appearing to indicate an initial rise of χ with increasing temperature followed by a plateau and a final decrease, although not all systems exhibit all stages. The aluminium and glass systems indicate, however, much steeper rises than the others, possibly due to the former involving specular reflections and the latter radiation transmission. Some effect of particle diameter is evident, with larger particle sizes appearing to sometimes result in smaller values of χ. Figure 7 indicates that if the particle diameter was doubled to change H_r from 10 to 20, say, then Y alters from about 12 to 17. However, experimental errors could result in $Y = 17 \pm 1$, say, for the latter and this would

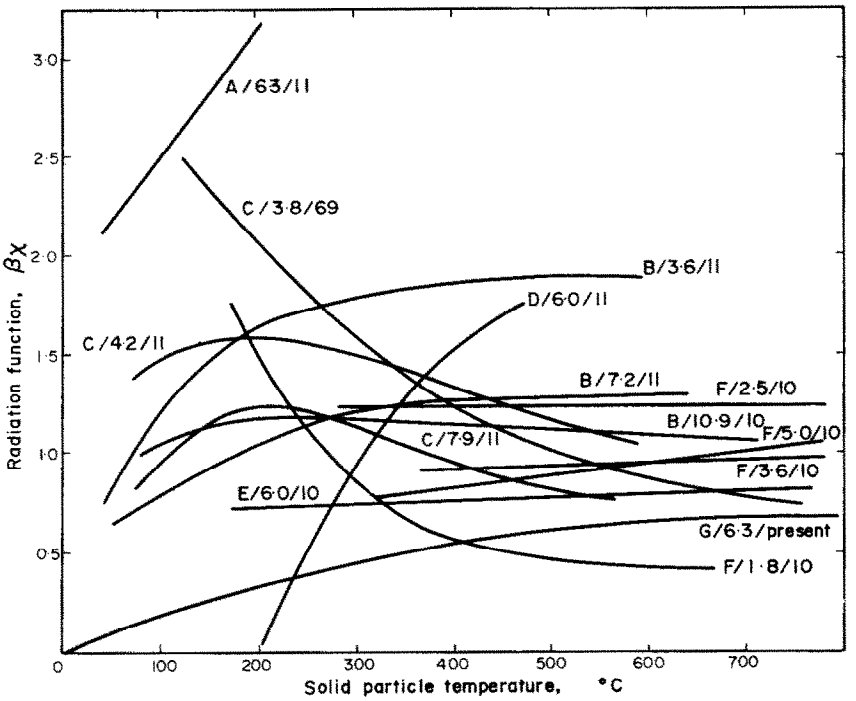

FIG. 13. The radiation function, χ, for stagnant beds of random packed spheres. Parameters refer to particle material, size of particle in mm and reference source. Material key: A—Aluminium, B—Steel, C—Alumina, D—Glass, E—Porcelain, F—Cement clinker, G—Alumina silicate.

represent an apparent increase or decrease in χ value for a larger particle, even although the trends in thermal conductivity and H_r values themselves were still consistent. Radiation scattering and emissivity variation can also contribute so that the observed trend with steel and aluminium may not be significant, and within the wide scatter of published results for different materials the effect of particle size would appear to be adequately accounted for by the present model. It would also seem from extrapolation of the majority of results that the original assumption of a negligible radiation contribution to heat flow is reasonable at 0°C.

As mentioned, some workers [11, 14, 69, 77] have evaluated the radiation contribution to packed bed heat transfer in terms of an effective radiation thermal conductivity, k_{e_r}, such that $Y = Y_c + Y_r$. Of doubtful validity due to an unrealistic separation of radiation into a parallel mechanism, this approach is followed here solely for the purpose of comparing the present experimental data with published models. Figure 14 compares the total thermal conductivity ratio, Y, for the present model and experimental results with the predictions of previous models which add the separate effective conduction and radiation thermal conductivities. Little agreement is found. The effective radiation thermal conductivity, k_{e_r}, can be obtained in the present case by subtracting the predicted conduction value from the experimental value of the effective thermal conductivity measurements (shown respectively by lines B and A of Fig. 3), and is presented as a ratio in Fig. 15. The predictions of previous radiation models cover a wide range of values, as also seen in these figures. The present model and experi-

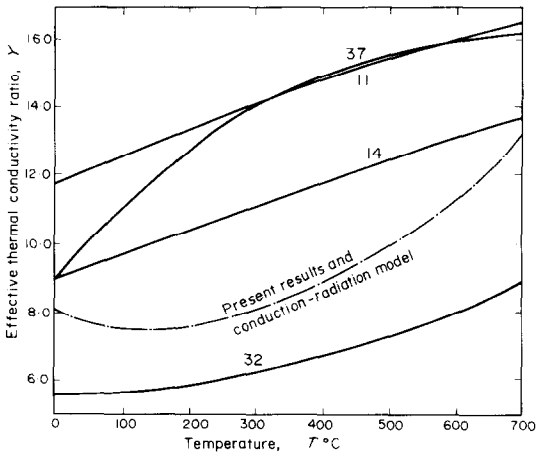

FIG. 14. Effective thermal conductivity ratio values ($Y = Y_c + Y_r$) for a stagnant bed compared with general model predictions. Parameters refer to reference source list.

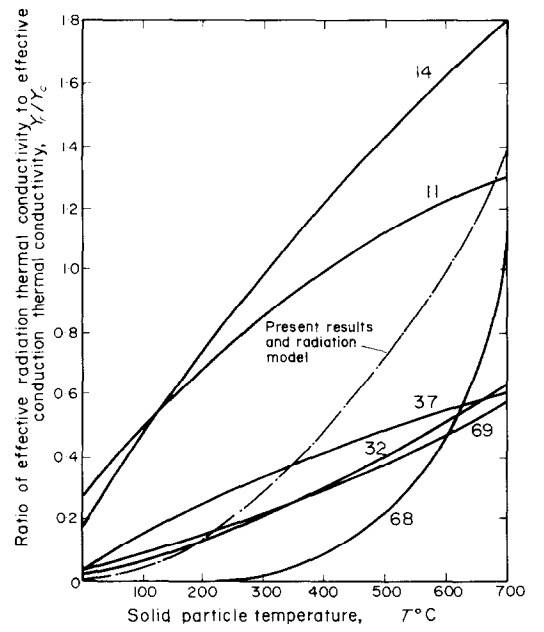

FIG. 15. The variation of the ratio of radiation to conduction heat transfer, Y_r/Y_c, for stagnant beds. Parameters refer to reference source list.

mental results lie near the middle of this range and show the expected increase due to radiation as the temperature increases. Once again the comparison brings out the wide variation of values given by different models.

6. CONCLUSIONS

Axial heat transfer in packed beds may be evaluated in terms of a number of model parameters which may each account for only one heat-transfer mechanism or which may lump together the effects of two or more mechanisms. From the comparison of the theoretical models and the experimental results it has been possible to build up a comprehensive picture of axial heat transfer for a stagnant bed.

For a stagnant bed a geometric model with no adiabatic boundaries within the solid phase was shown to effectively allow for flux line bending within the solid phase. This is particularly important under vacuum conditions which can be used to evaluate the contact area parameter. This model was extended to include inter-void and intra-void radiation at higher temperatures. While not new in its overall concept, the model does differ from previous proposals in some significant details to give a more realistic account of the mechanisms involved, basing these on fundamental parameters and correcting some previous inconsistencies and erroneous assumptions in the literature. The model for conduction alone is rigorously verified by comparison with published experimental measurements for which vacuum thermal conductivity values are available. When radiation is included in the model the situation becomes too complex to predict from fundamental considerations due to the unknown interaction of the view factor, emissivity factor, path length and effect of scattering which determine the value of the radiation parameter in the model. The present model, can, however, be successfully used if two experimental measurements are available to allow the point contact and the radiation parameter to be estimated.

The present analysis has indicated the wide disagreement between published predictions, but has allowed the estimation of the magnitude of the various mechanisms of heat transfer within a stagnant. bed. Final conclusions will be presented in Part II, where additional information on conduction and radiation contri-

butions can be derived from the gas flow investigations of packed bed heat transfer.

REFERENCES

1. R. SCHULTEN *et al.*, Physik der BBC-Krupp-Hochtemperaturreaktors, *Nukleonic* **1**(8), 277–286 (1959).
2. R. PRUSHEK, Der Transport von Wärme und Staff in der turbulent Strömung, *Forsch. Geb. Ing.* **29**(1), 11 (1963); **29**(2), 57 (1963).
3. ANON, Pebbles will produce power, *New Scientist* **27**, 143 (1965).
4. K. G. DENBIGH and G. S. G. BEVERIDGE, Oxidation of zinc sulphide spheres in an air stream, *Trans. Instn Chem. Engrs (London)* **40**(1), 23–34 (1962).
5. E. W. VOICE and R. WILD, A laboratory study of the sintering process, *J. Iron Steel Inst.* **183**, 404–410 (1956).
6. G. S. G. BEVERIDGE, The prediction of reaction zone propagation rates in beds of reacting solids, *Symposium on Chemical Engineering in the Metallurgical Industries*, Inst. Chem. Engrs, Proceedings, 87–104 (1963).
7. M. LEVA and M. GRUMMER, Heat transfer to gases through packed tubes. Effect of particle characteristics, *Ind. Engng Chem.* **40**, 415–419 (1948).
8. E. SINGER and R. H. WILHELM, Heat transfer in packed beds. Analytical solution and design method; fluid flow, solids flow and chemical reaction, *Chem. Engng Prog.* **46**, 343–357 (1950).
9. R. W. SCHULER, V. P. STALLINGS and J. M. SMITH, Heat and mass transfer in fixed bed reactor, *Chem. Engng Prog. Symp. Ser.* **48**, No. 4, 19–30 (1952).
10. S. YAGI and D. KUNII, Studies on effective thermal conductivities in packed beds, *A.I.Ch.E. Jl* **3**, 373 (1957).
11. R. F. BADDOUR and C. Y. YOON, Local radial effective conductivity and the wall effect in packed beds, *Chem. Engng Prog. Symp. Ser.* **57**, No. 32, 35 (1960).
12. W. B. ARGO and J. M. SMITH, Heat transfer in packed beds. Prediction of radial rates in gas solid beds, *Chem. Engng Prog.* **49**(8), 443–451 (1953).
13. D. KUNII and J. M. SMITH, Heat transfer characteristics of porous rocks, *A.I.Ch.E. Jl* **6**, 71 (1960).
14. W. SCHOTTE, Thermal conductivity of packed beds, *A.I.Ch.E. Jl* **6**(1), 63–67 (1960).
15. P. E. GLASER, *International Developments in Heat Transfer*, Part IV, p. 829. A.S.M.E. New York (1961).
16. D. P. HAUGHEY, Axial heat transfer in packed beds, Ph.D. Thesis, Edinburgh University (1966).
17. R. HAIGH, Morgan Refractories Ltd., Private Communication (1965).
18. D. P. HAUGHEY and G. S. G. BEVERIDGE, Local voidage variation in a randomly packed bed of equal-sized spheres, *Chem. Engng Sci.* **21**, 905–916 (1966).
19. D. P. HAUGHEY and G. S. G. BEVERIDGE, Property variations in a randomly packed bed of equal-sized spheres, *Chem. Engng Sci.* **22**, 715–718 (1967).
20. D. P. HAUGHEY and G. S. G. BEVERIDGE, Structural properties of packed beds—a review, *Can. J. Chem. Engng* **47**, 129–140 (1969).
21. K. LICHTENECKER, Dielectric constants of natural and artificial mixtures, *Physik. Z.* **27**, 115–158 (1926).
22. Y. ASAAD, Ph.D. Thesis, University of California (1955)
23. W. H. SOMERTON, *J. Petrol. Technol.* **10**(5), 61–64 (1958).
24. W. WOODSIDE and J. H. MESSMER, Thermal conductivity of porous media, I: Unconsolidated, *J. Appl. Phys.* **32**(9), 1688–1699 (1961).
25. G. T. TSAO, Thermal conductivity of two-phase materials, *Ind. Engng Chem.* **53**, 395–397 (1961).
26. S. C. CHENG and R. I. VACHON, Prediction of the thermal conductivity of two and three phase solid heterogeneous mixtures, *Int. J. Heat Mass Transfer* **12**, 249–264 (1969).
27. J. E. WARREN and J. H. MESSMER, Thermal conductivity of two-phase materials, *I/EC Fundamentals* **1**, 223 (1962).
28. R. G. DEISSLER and C. S. EIAN, Investigation of effective thermal conductivities of powders, Natl. Advisory Comm. Aeronaut., RM E52C05 (1952).
29. L. TOPPER, Analysis of porous thermal insulating materials, *Ind. Engng Chem.* **47**, 1377 (1955).
30. R. L. GORRING and S. W. CHURCHILL, Thermal conductivity of heterogeneous materials, *Chem. Engng Prog.* **57**(7), 53–59 (1961).
31. J. SHIMOKAWA, Deionization processes with ion exchange and with electromigration, Japan Atomic Energy Research Institute, JAERI 1038 (30 June 1962). Quoted in GODBEE and ZIEGLER [32].
32. H. W. GODBEE and W. T. ZIEGLER, Thermal conductivities of MgO, Al_2O_3 and ZrO_2 powders to 850°C, I: Experimental, *J. Appl. Phys.* **37**, 40–55, 56–65 (1966).
33. LORD RAYLEIGH, On the influence of obstacles arranged in rectangular order upon the properties of a medium, *Phil. Mag.* **34**, 481 (1892).
34. D. A. DE VRIES, Thermal conductivity of soil, *Mededel Landb. Hogesch. Wageningen* **52**, 1 (1952).
35. J. WEBB, Thermal conductivity of soil, *Nature* **177**, 989 (1956).
36. W. WOODSIDE, Calculation of the thermal conductivity of porous media, *Can. J. Phys.* **36**, 815–823 (1958).
37. G. N. DUL'NEV and Z. V. SIGALOVA, Thermal conductivity of granular systems, *Int. Chem. Engng* **5**, 218 (1965), also *J. Engng Phys. (USSR)* **7**(10), 49 (1961).
38. K. LICHTENECKER, Electrical resistance of aggregates, *Physik. Z.* **25**, 169–181, 193–204, 225–233 (1924).
39. H. W. RUSSELL, Principles of heat flow in porous insulators, *J. Am. Ceramic Soc.* **18**, 1–5 (1935).
40. T. E. W. SCHUMANN and V. VOSS, Heat flow through granulated material, *Fuel* **13**, 249–256 (1934).
41. J. C. MAXWELL, *A Treatise on Electricity and Magnetism*. 3rd ed., Vol. 1, p. 440. Clarendon Press, Oxford.
42. A. EUCKER, The thermal conductivities of ceramic refractory materials—Calculations of heat conductivity from its constituents, *Forsch. Geb. Ing.* **B3**, VDI-Forschungsheft, No. 353 (1932).
43. A. D. BRAILSFORD and K. G. MAJOR, The thermal conductivity of aggregates of several phases, including porous materials, *Br. J. Appl. Phys.* **15**, 313–319 (1964).
44. H. C. BURGERS, The conductivity of dilute alloys free from mixed crystals, *Physik. Z.* **20**, 73–75 (1919).
45. H. FRICKE, Electrical conductivity of a suspension of homogeneous spheroids, *Phys. Rev.* **24**, 575–587 (1924).
46. R. A. SEHR, The thermal conductivity of catalyst particles, *Chem. Engng Sci.* **9**, 145–152 (1958).
47. R. L. HAMILTON and O. K. CROSSER, Thermal conduc-

tivity of heterogeneous two-components systems, *I/EC Fundamentals* **1**, 187–191 (1962).
48. D. A. G. BRUGGEMAN, Dielectric constant and conductivity of mixtures of isotropic materials, *Ann. Physik.* **24**, 636–679 (1935).
49. W. VAN LOON, The gasification of carbon with oxygen and steam, Doctoral dissertation, Delft University (1952).
50. G. P. WILLHITE, D. KUNII and J. M. SMITH, Heat transfer in beds of fine particles (Heat transfer perpendicular to flow), *A.I.Ch.E. Jl* **8**, 340 (1962).
51. S. MASAMUNE and J. M. SMITH, Thermal conductivity of beds of spherical particles, *I/EC Fundamentals* **2**, 136–143 (1963).
52. H. G. KESSLER, Heat and mass transfer in freeze drying of porous media, *Chem. Ingr. Tech.* **34**, 163–171 (1962).
53. A. V. LUIKOV, A. G. SHASHKOV, L. L. VASILIEV and Y. E. FRAIMAN, Thermal conductivity of porous systems, *Int. J. Heat Mass Transfer* **11**, 117–140 (1968).
54. R. H. WILHELM, W. C. JOHNSON, R. WYNKOOP and D. W. COLLIER, Reaction rate, heat transfer and temperature distribution fixed bed catalytic convertors. Solution by electrical network, *Chem. Engng Prog.* **44**(2), 105–116 (1948).
55. G. H. M. WEBER RIEMANN, *Die Partiellen Differential-Gleichunger der Mathematischen Physik*, Band 1, p. 474. F. Vieweg and Sohn, Braunschweig (1919).
56. S. TAKEOKA and N. NAGASAKO, Heat transfer in a soldered bed, *Chem. Engng (Japan)* **27**, 646 (1963).
57. R. G. DEISSLER and J. S. BOEGLI, Investigation of effective thermal conductivities of powders in various gases, *Trans. Am. Soc. Mech. Engrs* **80**, 1417–1425 (1958).
58. E. H. KENNARD, *Kinetic Theory of Gases*. McGraw-Hill, New York (1938).
59. C. M. USISKIN and E. M. SPARROW, Thermal radiation between parallel plates separated by an absorbing-emitting non-isothermal gas, *Int. J. Heat Mass Transfer* **1**, 28–36 (1960).
60. R. VISKANTA and R. J. GROSH, *International Developments in Heat Transfer*, Part IV. A.S.M.E., p. 820 (1961); Heat transfer by simultaneous conduction and radiation in an absorbing medium, *Trans. Am. Soc. Mech. Engrs* **84C**, 63–72 (1962); Effect of surface emissivity on heat transfer by simultaneous conduction and radiation, *Int. J. Heat Mass Transfer* **5**, 729 (1962); *Appl. Mech. Revs.* **17**, 91 (1964).
61. R. VISKANTA, Heat transfer in a radiating fluid with flood flow in a parallel plate channel, *Appl. Sci. Res.* **13A**, 291–311 (1964).
62. M. A. HEASLET and R. F. WARMING, Radiative transport and wall temperature slip in an absorbing planar medium, *Int. J. Heat Mass Transfer* **8**, 979–994 (1965).
63. J. R. HOWELL, Determination of combined conduction and radiation of heat through absorbing media by the exchange factor approximation, *Chem. Engng Prog. Symp. Ser.* **61**, No. 59, 162–171 (1965).
64. S. C. TRAUGOTT and K. C. WANG, On differential methods for radiant heat transfer, *Int. J. Heat Mass Transfer* **7**, 269–272 (1964).
65. H. C. HOTTEL, Radiation as a diffusion process, *Int. J. Heat Mass Transfer* **5**, 82, 559 (1962).
66. H. C. HAMAKER, Radiation and heat conduction in light scattering material, *Philips Res. Rep.* **2**, 55–67, 103–111, 112–125, 420–425 (1947).
67. B. K. LARKIN and S. W. CHURCHILL, Heat transfer by radiation through porous insulations, *A.I.Ch.E. Jl* **5**, 467–474 (1959), also B. K. LARKIN, Rate of thermal radiation through porous insulating materials, Ph.D. Thesis, University of Michigan (1957).
68. J. C. CHEN and S. W. CHURCHILL, Radiant heat transfer in packed beds, *A.I.Ch.E. Jl* **9**, 35–41 (1963), also J. C. CHEN, Ph.D. Thesis, University of Michigan (1961).
69. F. B. HILL and R. H. WILHELM, Radiative and conductive heat transfer in a quiescent gas-solid. Bed of particles: theory and experiment, *A.I.Ch.E. Jl* **5**, 486–496 (1959), also F. B. HILL, Ph.D. Thesis, Princeton University (1958).
70. R. C. L. BOSWORTH, *Heat Transfer Phenomena*. Pergamon Press, Oxford (1952).
71. R. W. POWELL, Experiments using a simple thermal comparator for measurement of thermal conductivity, surface roughness and thickness of foils or of surface deposits, *J. Scient. Instrum.* **34**, 485–492 (1957); *Mem. Sci. Rev. Metall.* **56**, 181 (1959); *Bull. de l'Inst. Intl. du Froid*, Annex 1960–2, p. 129.
72. W. T. CLARK and R. W. POWELL, Measurement of thermal conduction by the thermal comparator, *J. Scient. Instrum.* **39**, 545–551 (1962).
73. S. WOLOGDINE and A. L. QUENEAU, Conductivity, porosity and gas permeability of refractory material, *Chem. Met. Engng* **7**, 383, 433 (1909).
74. I. GLASSMANN and C. F. BONILLA, Thermal conductivity and Prandtl number of air at high temperature, *Chem. Engng Prog. Symp. Ser.* **49**, No. 5, 153 (1953).
75. W. G. KANNULUIK and L. H. MARTIN, Conduction of heat in powders, *Proc. R. Soc., Lond.* **A141**, 144–158 (1933).
76. M. PIRANI, Radiation properties of different substances within the temperature range 250°C–800°C, *J. Scient. Instrum.* **16**, 372 (1939).
77. G. DAMKOHLER *Der Chemie Ingenieur*, Vol. 3, p. 441. Akademische Verlagsgesellschaft, Leipzig (1937).
78. R. A. FISCHER, On the capillary forces in an ideal soil: Correction of formulae given by W. B. Haines, *J. Agr. Sci.* **16**, 492–505 (1926).
79. W. J. ROSE, Volumes and surface areas of pendular rings, *J. Appl. Phys.* **29**, 687–691 (1958).
80. F. A. JENKINS and H. E. WHITE, *Fundamentals of Optics*, pp. 455. McGraw-Hill, New York (1957).
81. N. WAKAO, K. KATO and N. FURUYA, New factor between two hemispheres in contact and radiation heat-transfer coefficient in packed beds, *Int. J. Heat Mass Transfer* **12**, 118–120 (1969).

APPENDICES

Conduction and Radiation Models for One-Dimensional Packed Bed Heat Transfer

This geometric model for the packed bed effective thermal conductivity, k_e, is based on an idealized arrangement of gas and solid phases. A simple one-dimensional representa-

tion, it is suitable for describing both conduction and conduction/radiation mechanisms.

The bed is considered to consist of an assembly of unit cells, built up of columns of cells placed on top of each other, and the columns arranged side by side in the direction of heat flow such that a cross-sectional slice through the bed has a bulk mean voidage equivalent to that in the bed. The unit cell (Fig. 4f) has a unit cross-sectional area, a thickness or height equivalent to the layer spacing, βD_p, (defined as the distance between particle centres in adjacent layers [18]) and contains a fractional volume $(1 - \varepsilon)$ of solid material of thermal conductivity, k_s, and volume ε of stagnant gas of conductivity, k_g. The side boundaries of the cell are assumed to be adiabatic while the top and base planes are considered as isothermal with a temperature drop ΔT between them.

Appendix 1: Conduction Model

The unit cross-sectional area is divided into three parallel paths of areas ε_{A_1}, ε_{A_2} and ε_{A_3}. Conduction in the bulk gas (mechanism 2) will take place over the full cell length, βD_p, and area ε_{A_1} at a heat flow rate, Q_1, per unit area given by

$$Q_1 = k_g \varepsilon_{A_1} \Delta T / \beta D_p. \tag{A.1}$$

Conduction through the solid (mechanism 1) will have a path length $(\beta - \phi)D_p$ over an area $(\varepsilon_{A_2} + \varepsilon_{A_3})$ and will be in series with the parallel mechanisms (4 and 3) of contact point conduction over a length ϕD_p and area ε_{A_3} and conduction in the surrounding gas over a length ϕD_p and area ε_{A_2}. If ΔT_1 and ΔT_2 are the respective temperature drops, then mechanism 1 will account for a heat flux

$$Q_2 = \frac{k_s(\varepsilon_{A_2} + \varepsilon_{A_3})\,\Delta T_1}{(\beta - \phi)D_p}$$

and while for the combined mechanisms 3 and 4 it will be

$$Q_{3/4} = \frac{k_g \varepsilon_{A_2} + k_s \varepsilon_{A_3}}{\phi D_p} \Delta T_2 . \tag{A.2}$$

Since $\Delta T = \Delta T_1 + \Delta T_2$ and $Q_2 = Q_{3/4}$ we get

$$Q_2 = \frac{\Delta T}{D_p} \Bigg/ \left[\frac{\beta - \phi}{k_s(\varepsilon_{A_2} + \varepsilon_{A_3})} + \frac{\phi}{k_g \varepsilon_{A_2} + k_s \varepsilon_{A_3}} \right]. \tag{A.3}$$

The total heat flow through the cell, Q, is

$$Q = \frac{k_{e_c} \Delta T}{\beta D_p} = Q_1 + Q_2$$

so that the desired expression for the thermal conductivity is

$$k_{e_c} = \varepsilon_{A_1} k_g + \beta \Bigg/ \left[\frac{\beta - \phi}{k_s(\varepsilon_{A_2} + \varepsilon_{A_3})} + \frac{\phi}{k_g \varepsilon_{A_2} + k_s \varepsilon_{A_3}} \right]$$

or in dimensionless form

$$Y_c = \varepsilon_{A_1} + \frac{1}{\dfrac{1 - \alpha}{X(1 - \varepsilon_{A_1})} + \dfrac{\alpha}{\varepsilon_{A_2} + X\varepsilon_{A_3}}} \tag{A.4}$$

where $Y_c = k_{e_c}/k_g$, $X = k_s/k_g$, $\alpha = \phi/\beta$. This reduces under vacuum conditions to

$$Y_c^* = X \Bigg/ \left[\frac{1 - \alpha}{1 - \varepsilon_{A_1}} + \frac{\alpha}{\varepsilon_{A_3}} \right]. \tag{A.5}$$

It can be easily shown that the thermal conductivity for the cell is equivalent to that for a bed composed of an assembly of cells.

Appendix 2: Evaluation of Conduction Model Parameters

It remains to evaluate the various parameters ε_{A_1}, ε_{A_2} and ε_{A_3}, and $\alpha = \phi/\beta$.

The number of points of contact, n, on a particle can be simply represented by the expression

$$n = 22{\cdot}47 - 39{\cdot}39\varepsilon$$

where ε is the bulk mean voidage of the bed [18]. It is assumed that the volume of gas associated with mechanism 3 equals the volume of pendular gas rings surrounding each contact point between particles in the cell. These rings are assumed to cover the maximum possible surface area of each particle, a condition obtained when the contact points are equispaced from each other and adjacent rings touch. The pendular ring angle, θ_{PR}, is half the angle subtended at the centre of a particle by the circumference of a ring touching the particle surface and from the latter assumption it can be shown [18] that

$$\theta_{PR} = \tfrac{1}{2} \cos^{-1} \left[\frac{\cos \pi n/3(n - 2)}{1 - \cos \pi n/3(n - 2)} \right].$$

Fischer [78] and Rose [79] have shown that the volume of a pendular ring is

$$V_{PR} = \frac{\pi D_p^3}{4} (\sec \theta_{PR} - 1)^2 \left[1 - \left(\frac{\pi}{2} - \theta_{PR} \right) \tan \theta_{PR} \right].$$

The number of contacts and hence the number of pendular rings, N_{PR}, within a unit cell is

$$N_{PR} = \frac{n}{2} \beta D_p \frac{6(1 - \varepsilon)}{\pi D_p^3} \tag{A.6}$$

since for a cell volume βD_p, the fractional volume of solid is $1 - \varepsilon$, the volume of one sphere is $\pi D_p^3/6$, and each of the contact points on a sphere is associated with two particles. The gas volume in the series path is

$$\phi D_p \varepsilon_{A_2} = N_{PR} V_{PR}.$$

Therefore

$$\alpha = \frac{\phi}{\beta} = \frac{3(1 - \varepsilon)n}{4\varepsilon_{A_2}} (\sec \theta_{PR} - 1)^2 \left[1 - \left(\frac{\pi}{2} - \theta_{PR} \right) \tan \theta_{PR} \right]$$

which can be written for convenience as $\alpha = \alpha^*/\varepsilon_{A_2}$. We are now in a position to find the term represented by α^*.

Since the total gas volume in the cell is $\varepsilon\beta D_p = \varepsilon_{A_1}\beta D_p + \varepsilon_{A_2}\phi D_p$ and $\beta = \phi/\alpha$, then $\varepsilon = \varepsilon_{A_1} + \varepsilon_{A_2}\alpha = \varepsilon_{A_1} + \alpha^*$ so that $\varepsilon_{A_1} = \varepsilon - \alpha^*$. Since $\varepsilon_{A_1} + \varepsilon_{A_2} + \varepsilon_{A_3} = 1$ we then get $\varepsilon_{A_2} + \varepsilon_{A_3} = 1 - \varepsilon + \alpha^*$.

If the contact area, ε_{A_3}, is negligible the parameters are now completely defined. Normally, however, ε_{A_3} canot be neglected. Since ε_{A_3} is a function of particle surface characteristics, solid elasticity and particle loading it cannot be evaluated solely from the bed geometry but must be obtained from an experimental effective thermal conductivity measurement under the required particle surface and loading conditions. The experimental measurement may be made either under vacuum or at atmospheric pressure at a temperature such that radiation effects are insignificant, and ε_{A_3} obtained from equations (A.5) or (A.4) respectively.

An alternative form for ε_{A_3} is in terms of the contact point area angle, θ_p. If ε_{A_3} is assumed to be composed of a circular area of contact at each contact point within the unit cell, then a contact area angle θ_P may be evaluated. This angle is defined as half the angle subtended at a sphere centre by the circumference of the contact area at each contact point. Thus it follows that

$$N_{PR}\pi\left(\frac{D_p}{2}\sin\theta\right)^2 = \varepsilon_{A_3}$$

and, from equation (A.6), that

$$\theta_p = \sin^{-1}\left[\frac{4\varepsilon_{A_3}}{3(1-\varepsilon)\beta n}\right].$$

Appendix 3: Conduction—Radiation Model

As the radiation mechanisms act along the gas conduction paths, they can be added to the basic conduction model.

Radiation between adjacent particle surfaces (mechanism 5) can be accounted for by the application of a radiation heat-transfer coefficient, h_{r_s}, over the area ε_{A_2} of the solid–gas interface in the series path (Fig. 4f). The heat flux given by equation (A.2) then becomes

$$Q_{3/4} = \left[\frac{k_g\varepsilon_{A_2} + k_s\varepsilon_{A_3}}{\phi D_p} + h_{r_s}\varepsilon_{A_2}\right]\Delta T_2$$

so that equation (A.3) becomes

$$Q_2 = \frac{\Delta T}{D_p}\Big/\left[\frac{\beta-\phi}{k_s(\varepsilon_{A_2}+\varepsilon_{A_3})} + \frac{\phi}{\varepsilon_{A_2}(k_g + h_{r_s}\phi D_p) + k_s\varepsilon_{A_3}}\right].$$

Radiation between surfaces seen through more than one void (mechanism 6) can be represented by the use of a coefficient h_{r_g} used over the area ε_{A_1}. Then equation (A.1) for the gas parallel path the heat flux becomes

$$Q_1 = \varepsilon_{A_1}(k_g + h_{r_g}\beta D_p)\,\Delta T/\beta D_p.$$

(This mechanism could be achieved physically in the model by rotating alternative unit cells in any one column through 180°.)

It then follows that

$$k_e = \varepsilon_{A_1}k_g\left[1 + \frac{h_{r_g}\beta D_p}{k_g}\right] + \beta\Big/\left[\frac{\beta-\phi}{k_s(\varepsilon_{A_2}+\varepsilon_{A_3})} + \frac{\phi}{\varepsilon_{A_2}(k_g + h_{r_s}\phi D_p) + k_s\varepsilon_{A_3}}\right]$$

or, writing $H_{r_g} = h_{r_g}\beta D_p/k_g$ and $H_{r_s} = h_{r_s}\beta D_p/k_g$,

$$Y = \varepsilon_{A_1}(1 + H_{r_g}) + 1\Big/\left[\frac{1-\alpha}{X(1-\varepsilon_{A_1})} + \frac{\alpha}{\varepsilon_{A_2}(1+\alpha H_{r_s}) + X\varepsilon_{A_3}}\right]. \quad \text{(A.7)}$$

Appendix 4: Evaluation of Radiation Model Parameters

The area fractions ε_{A_1}, ε_{A_2}, ε_{A_3} are evaluated from the conduction model: It remains to evaluate the radiation parameters H_{r_g} and H_{r_s}.

Of the three types of radiation, transmission through the solid material of the particle need only be considered when the solid is not opaque to radiation, as is the case for glass [68]. Scattering occurs when electromagnetic waves encounter a discontinuity in refractive index. In particular, forward scattering of backward radiation increases heat transfer when radiation hits a solid with dimensions smaller than the radiation wavelength [15, 80], an effect which can be significant in packed bed systems [61, 68]. The third mode of radiation, namely absorption-emission, satisfies a relation of the form $Q = \sigma\chi T^4$ where σ is the Stefan–Boltzmann constant, T the absolute temperature, and χ a radiation function involving a function of emissivity, e, a view factor. Although packed beds can be taken as gray surfaces and assumed to emit radiation diffusely (except for very smooth surfaces with unsymmetrical specular reflection [11], both the view factor and emissivity will be functions of temperature. The view factor, defined as the fraction of radiation leaving one surface received by another, is affected by scattering. The expression for heat flux may thus be replaced by

$$Q = \sigma\chi(T_1^4 - T_2^4) = h_r(T_1 - T_2)$$

to define the radiation coefficient, h_r, which has the approximate form $h_r = 4\sigma\chi T^3$. The emissivity function contribution to the radiation function takes various forms, for example

$$\left[\frac{1}{e_1} + \frac{A_1}{A_2}\left(\frac{1}{e_2} - 1\right)\right]^{-1}$$

which reduces for two parallel plates of the same material to $e/(2-e)$. Other forms such as εe [77], $e^2/2$ [37], e [14], $w^2e[(1/1-\varepsilon) - 1]$ where w is the gas refractive index [32],

$$2\Big/\left[\frac{2}{e} - 0{\cdot}264\right] \quad [81]$$

and

$$\left[1 + \frac{\varepsilon(1-e)}{2e(1-\varepsilon)}\right]^{-1} \quad [10]$$

have been suggested based upon different assumptions as to the solid geometry.

Attempts have been made to distinguish between the bed mechanisms 5 and 6 but this is unlikely to lead to much improvement without going to the more complex models outlined earlier.

Due to unknown view factors, emissivity factors, temperature dependence and radiation scattering factors it does not appear possible to evaluate the radiation parameters solely from the geometry of the model and they must be obtained by fitting a model to experimental thermal conductivity measurements made at temperatures such that radiation is significant. Since these parameters will be functions of temperature, it is not feasible to distinguish between them. In equation (A.7) it is thus assumed that $h_r = h_{r_g} = h_{r_s}$ and hence $H_r = H_{r_g} = H_{r_s}$. This assumption will provide a good approximation in practice since the value of the fractional series gas layer thickness α is small (of the order of 10 per cent), reducing any error in taking $h_{r_g} = h_{r_s}$. Equation (A.7) would then be used to evaluate H_r at different temperature levels, after initially obtaining the conduction parameters at a sufficiently low temperature.

TRANSFERT THERMIQUE AXIAL DANS LES GARNISSAGES LITS FIXES ENTRE 20 ET 700°C

Résumé—De nombreuses applications industrielles de garnissages formés de particules solides rangées au hasard impliquent un transfert thermique axial et à haute température.

On a estimé les mécanismes de conduction et rayonnement indépendamment des effects convectifs pour de tels systèmes en utilisant un modèle géométrique qui tient compte de la courbure des lignes de flux dans la phase solide. Ce modèle a été utilisé pour analyser des mesures expérimentales de transfert thermique dans un lit fixe de billes de silicate d'aluminium pour le domaine de température de 20 à 750°C. On a aussi effectué des comparaisons avec d'autres modèles théoriques et d'autres résultats expérimentaux.

AXIALE WÄRMEÜBERTRAGUNG IN FESTBETTEN, FESTBETTEN ZWISCHEN 20 UND 750°C

Zusammenfassung—Viele industrielle Anwendungen von beliebig gepackten Festbetten für feste Teilchen berühren das Gebiet der axialen Wärmeübertragung bei hohen Temperaturen.

Die Mechanismen der Wärmeleitung und -strahlung wurden für solche Systeme unabhängig von konvektiven Effekten entwickelt, wobei ein modifiziertes geometrisches Modell benutzt wurde unter Berücksichtigung der Stromlinien, die in der festen Phase gekrümmt sind. Benutzt wurde dieses Modell zur Analyse experimenteller Messungen der Wärmeübertragung in Festbetten aus trägen Aluminium-Silikat-Kugeln über einen Temperaturbereich von 20 bis 750°C. Vergleiche mit anderen theoretischen Modellen und experimentellen Daten wurden angestellt.

АКСИАЛЬНЫЙ ТЕПЛООБМЕН В ПЛОТНЫХ СЛОЯХ. НЕПОДВИЖНЫЕ СЛОИ ПРИ ТЕМПЕРАТУРАХ ОТ 20 ДО 750°С

Аннотация—Многие случаи промышленного использования произвольных плотных слоев твердых частиц включают аксиальный высокотемпературный теплообмен. Механизм кондуктивного и радиационного теплообмена оценивался для таких систем независимо от конвективных эффектов с использованием модифицированной геометрической модели, которая учитывает изгиб линий тока в твердой фазе. Эта модель использовалась для анализа экспериментальных данных по теплообмену в неподвихном слое инертных алюмо-силикатных шариков в диапазоне температур от 20 до 750°С. Проведено также сравнение с другими теоретическими моделями и экспериментальными данными.